Journal of Inflammation Research

Dovepress
Taylor & Francis Group

Open Access Full Text Article

ORIGINAL RESEARCH

Identification and Experimental Validation of PANoptosis-Related Genes in Idiopathic Pulmonary Fibrosis by Bioinformatics Analysis

Dongguang Wang[1,2,*], Yifan Yuan[3–5,*], Xiang Tong[1,2], Lian Wang[1,2], Jibo Sun[1,2], Shijie Zhang[1,2], Sitong Liu[1,2], Huatian Gan[3–5], Hong Fan[1,2]

[1]Department of Respiratory and Critical Care Medicine, and National Clinical Research Center for Geriatrics, West China Hospital, Sichuan University, Chengdu, People's Republic of China; [2]State Key Laboratory of Respiratory Health and Multimorbidity, West China Hospital, Sichuan University, Chengdu, People's Republic of China; [3]Center of Gerontology and Geriatrics, West China Hospital, Sichuan University, Chengdu, People's Republic of China; [4]Centre for Inflammatory Bowel Disease, West China Hospital, Sichuan University, Chengdu, People's Republic of China; [5]Lab of Inflammatory Bowel Disease, Frontiers Science Center for Disease-Related Molecular Network, West China Hospital, Sichuan University, Chengdu, People's Republic of China

*These authors contributed equally to this work

Correspondence: Huatian Gan, Center of Gerontology and Geriatrics, West China Hospital, Sichuan University, No. 37 Guoxue Alley, Chengdu, 610041, People's Republic of China, Email ganhuatian123@163.com; Hong Fan, Department of Respiratory and Critical Care Medicine, National Clinical Research Center for Geriatrics, West China Hospital, Sichuan University, No. 37 Guoxue Alley, Chengdu, 610041, People's Republic of China, Email fanhong@scu.edu.cn

Aim: To identify the molecular signature of differentially expressed genes (DEGs) associated with PANoptosis in idiopathic pulmonary fibrosis (IPF) and to interpret their immune landscape and cellular distribution characteristics.

Methods and Results: We acquired two IPF datasets from the Gene Expression Omnibus (GEO) database to identify PANoptosis-related DGEs (PAN-DEGs), initially identifying thirty PAN-DEGs. Utilizing machine learning algorithms, we established a five-gene PANoptosis-related signature comprising IGF1, GPX3, GADD45β, SMAD7, and TIMP3, each demonstrating robust diagnostic performance. The expression of these hub genes was subsequently validated using a third GEO dataset and a bleomycin-induced pulmonary fibrosis model. Immune infiltration analysis revealed a close association of these genes with various immune cells, and single-cell RNA sequencing indicated significant expression changes in diverse pulmonary cell types, particularly endothelial cells and fibroblasts.

Conclusion: We identified and validated a PANoptosis-related gene signature in IPF, providing insights into their immune infiltration and potential cellular distribution. Further research is necessary to elucidate the biological functions and mechanisms of these genes in the pathogenesis of IPF.

Keywords: bioinformatics analysis, differentially expressed genes, idiopathic pulmonary fibrosis, PANoptosis

Introduction

Idiopathic pulmonary fibrosis (IPF) represents a significant progressive fibrotic lung disease with an unknown etiology. It is characterized by persistent physiological impairment, deteriorating respiratory symptoms, and reduced pulmonary function.[1] The progression and prognosis of IPF are typically unpredictable and vary among individuals. In patients not receiving anti-fibrotic therapies, the average survival period is approximately four years.[2] In recent decades, increased awareness of IPF has led to notable advancements in treatment regimens, while the overall prognosis remains largely unchanged. Consequently, a deeper understanding of the cellular processes and molecular mechanisms involved is crucial for the development of effective treatments.

Programmed cell death (PCD) is an autonomous and orderly form of cell death that plays a critical role in maintaining health and contributing to human disease.[3] It generally involves common fundamental components that lead to the spontaneous termination of a cell due to developmental cues or immune-mediated signals initiated by death receptors.[4]

Received: 25 November 2024
Accepted: 1 April 2025
Published: 23 April 2025

Numerous PCDs have been identified in mammalian cells with apoptosis, pyroptosis, and necroptosis being the three primary types. These PCDs form distinct individual pathways while also contributing to a highly interconnected and coordinated cell death system.[5] The significance of these PCDs in tissue damage and fibrotic remodeling associated with IPF has been documented in some studies.[6–8] However, medications targeting PCDs have not yet demonstrated success in clinical trials. PANoptosis, a unique inflammatory PCD modality initially identified in the context of infectious diseases, integrates key features of apoptosis, pyroptosis, and necroptosis. It is regulated by a polymeric protein complex that senses pathogens, pathogen-associated molecular patterns, damage-associated molecular patterns (DAMPs), and cytokines.[9] Recent research has demonstrated that PANoptosis also plays a role in the development of pulmonary diseases, including septic lung injury and acute respiratory distress syndrome (ARDS).[10,11] A latest study found that the traditional Chinese medicine can delay the progression of bleomycin-induced pulmonary fibrosis by inhibiting PANoptosis, suggesting its involvement in pulmonary fibrosis.[12] Nevertheless, the primary targets of signaling pathways mediated by PANoptosis remain inadequately defined.

The application of innovative bioinformatic tools is expediting research into the pathogenesis of IPF, thereby enhancing our understanding of the disease's pathways, cell-specific mechanisms, and cell-cell interactions that contribute to the fibrotic environment.[13] In this study, we performed a comprehensive bioinformatic analysis to elucidate the role of PANoptosis in the pathogenesis of pulmonary fibrosis and to identify key genes that regulate PANoptosis-mediated cellular processes. Initially, gene expression profiles from IPF patients and normal controls were retrieved from the Gene Expression Omnibus (GEO) database,[14] and PANoptosis-related differentially expressed genes (DEGs) were identified using Weighted Gene Co-expression Network Analysis (WGCNA).[15] Subsequently, key candidate signatures were identified through machine learning techniques. These PANoptosis-related candidate genes were then validated using two external datasets, and a nomogram model was employed to predict the risk of IPF. In addition, we developed a bleomycin-induced murine model of pulmonary fibrosis to further validate the expression of these genes. Finally, the distribution of hub genes was analyzed through immune infiltration and single-cell analyses. This study aims to investigate the potential mechanisms of PANoptosis in IPF and to propose a viable therapeutic strategy for this irreversible condition.

Materials and Methods

The Acquisition of Datasets and Processing

The "GEOquery" R package was used to get gene expression of IPF patients and healthy controls from the GEO database (https://www.ncbi.nlm.nih.gov/geo/). The GSE32537 dataset contained 167 fibrosing idiopathic interstitial pneumonia and 50 non-disease control lung tissues, which were performed on the GPL6244 platform. GSE47460 included sequencing data of 206 UIP/IPF and 108 control lung tissues, which were performed on the GPL6480 and GPL14550 platforms. The Bioconductor "sva" R package was used for removing batch effects and making a unified GEO dataset. An external validation was conducted using the GSE110147 dataset performed on the GPL6244 platform, of which lung tissue samples were obtained from 22 IPF patients and 11 normal controls. All data were transformed into logarithmic form for subsequent analyses. The workflow chart was illustrated in Figure 1.

Identification of Differentially Expressed Genes and Candidate Key PANoptosis-Related DEGs (PAN-DEGs)

To identify DEGs, we conducted Principal Component Analysis (PCA) using the "FactoMineR" and "factoextra" R packages, and differential analysis using the "Limma" package, with a threshold of adjusted P value < 0.05 and $|\text{fold change}| \geq 0.5$. Visualization of DEGs between IPF and controls was achieved through a volcano plot using "ggplot2" and a heatmap using the "pheatmap" package. The PANoptosis gene set integrated genes associated with apoptosis, pyroptosis, and necroptosis. We combined the Molecular Signature Database (MsigDB) version 7.0 (http://www.gsea-msigdb.org/gsea/msigdb/) with the PANoptosis-related genes reported in a previous study,[16] to produce a comprehensive PANoptosis-related gene set. After duplication, 274 key candidate genes were remained and used for the subsequent analyses. Detailed PANoptosis-related genes were shown in Supplementary Table 1.

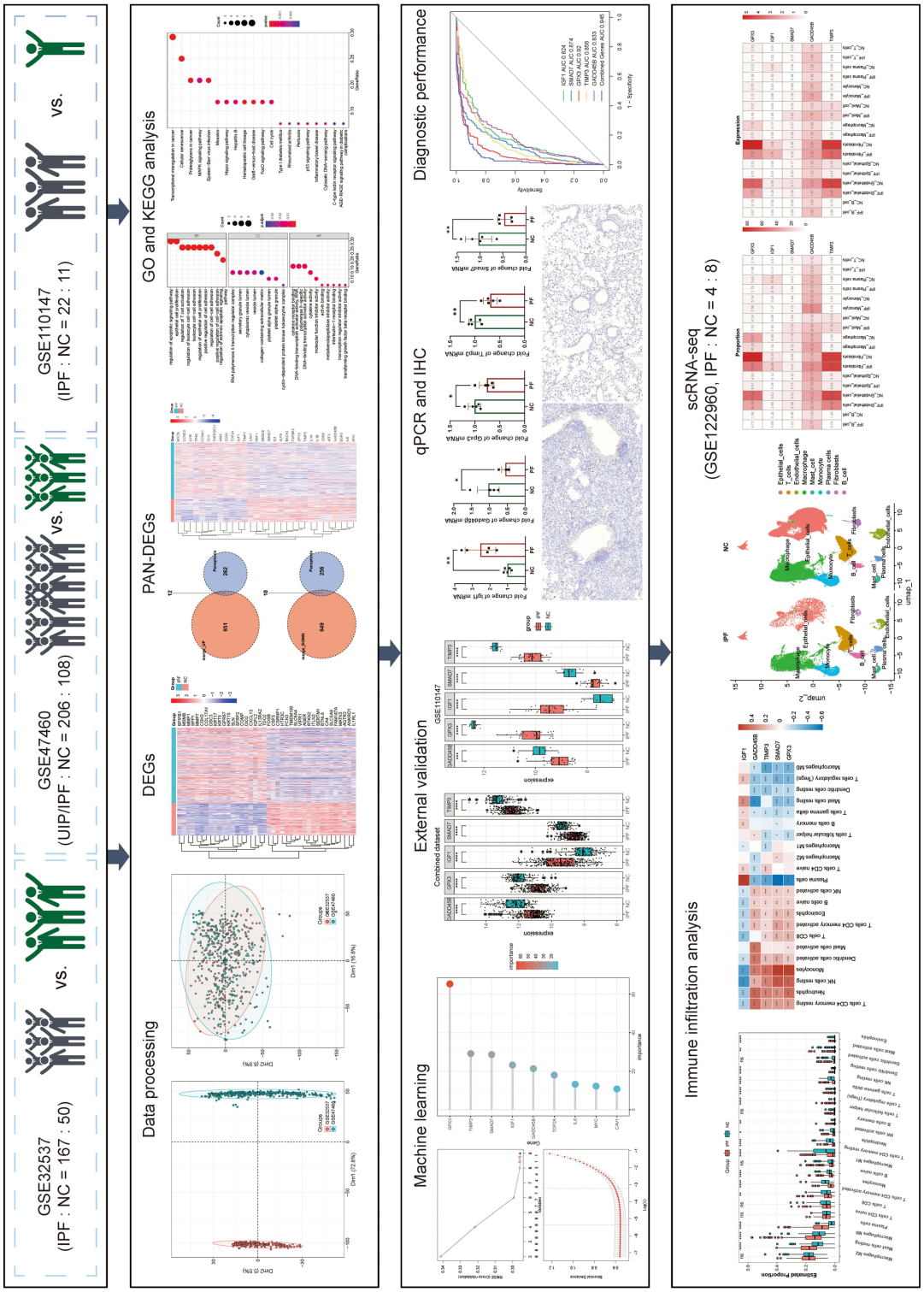

Figure 1 Schematic representation of the workflow for the study.

https://doi.org/10.2147/JIR.S505229

Functional Enrichment Analysis of DEGs and PAN-DEGs in IPF

Further investigation of biological functions of identified DEGs were conducted with Gene Ontology (GO) enrichment and Kyoto Encyclopedia of Genes and Genomes (KEGG) pathway analyses, using the R package of "clusterProfiler".

WGCNA

We employed WGCNA using the "WGCNA" R package to identify gene modules associated with IPF. Normalized expression data from IPF patients and controls were filtered to remove low-variance genes. A weighted gene co-expression network was constructed with a soft-thresholding power to achieve scale-free topology. The adjacency matrix was converted into a topological overlap matrix to measure network connectivity, and gene modules were identified using hierarchical clustering. Modules were defined by branches of the dendrogram and assigned unique colors. Module eigengenes were correlated with clinical traits, and significant modules were identified. Candidate hub genes within these modules were determined using a module membership threshold of > 0.8 and intersected with previously identified PANoptosis-related differentially expressed genes. Visualization of the dendrogram, module colors, and module-trait relationships illustrated the associations. Detailed hub genes in each module were shown in Supplementary Table 2.

Protein-Protein Interaction (PPI) Network Analysis

We used GeneMANIA (http://genemania.org/) to construct a PPI network for candidate hub PANoptosis-related genes.[17] This tool integrates data from various sources such as physical interactions and co-expression. Default settings were applied, and interactions were prioritized based on confidence scores. The network visualization displayed nodes as genes/proteins and edges as interactions, with thickness and color indicating interaction confidence. Key hub genes with high interaction counts were identified, highlighting their potential roles in IPF pathogenesis and relevance as therapeutic targets or biomarkers.

Machine Learning

We employed machine learning methods to select and reduce the dimensions of candidate genes derived from WGCNA modules and previously identified PAN-DEGs. Gene expression data were standardized and divided into training and test sets for cross-validation. Feature selection was performed using SVM-RFE (Support Vector Machine - Recursive Feature Elimination) with the R package "e1071" to pinpoint the most discriminative genes. Additionally, Random Forest was utilized to rank genes based on their importance scores using the R package "randomForest".[18] To further refine the gene selection, LASSO regression was applied with the R package "glmnet", with the optimal λ chosen based on the minimum binomial deviance.[19] The selection process was evaluated and optimized through cross-validation to ensure robustness. This comprehensive approach enabled the identification of hub genes, setting the stage for further functional analysis and offering insights into the molecular mechanisms underlying IPF.

Validation and Functional Analysis of Hub Genes

To validate and analyze the functional roles of key genes identified through machine learning techniques, we assessed gene expression levels in both a combined dataset and an independent validation dataset (GSE110147). Boxplots were generated using the "ggplot2" R package to compare expression between IPF patients and normal controls, confirming significant differential expression. We performed pathway enrichment analysis using the HALLMARK gene sets from the Molecular Signature Database (MsigDB) version 7.0 (http://www.gsea-msigdb.org/gsea/msigdb/) to explore the biological functions of the key genes. Correlations between the key genes and various biological pathways were visualized with a heatmap using the "ComplexHeatmap" R package, highlighting significant associations. The interactions among the key genes were illustrated using a chord diagram created with the "circlize" R package, demonstrating their co-regulation and potential combined effects in IPF. The diagnostic potential of the key genes was evaluated using Receiver Operating Characteristic (ROC) curves with the "pROC" R package, and the area under the curve (AUC) values were calculated to assess their accuracy in distinguishing IPF patients from normal controls.

Immune Cell Infiltration Analysis

To understand the immunological mechanisms underlying IPF and its association with hub gene expressions, we utilized the CIBERSORT algorithm to estimate the fractions of 22 immune cell types in both IPF patients and normal controls. Gene expression profiles were input into CIBERSORT, which provided relative proportions of immune cell types in each sample. The resulting data were visualized using violin plots created with the "ggplot2" R package to compare the distribution of immune cell fractions between IPF patients and normal controls, with statistical significance assessed using the Wilcoxon rank-sum test. To investigate the relationship between hub gene expressions and immune cell fractions, Pearson correlation coefficients were calculated and visualized with a heatmap using the "ComplexHeatmap" R package. Significant correlations were marked by asterisks, indicating robust associations between gene expression and immune cell infiltration. Gene set variation analysis (GSVA) is an unsupervised gene set enrichment analysis method used to evaluate changes in gene set activity in a single sample. It directly calculates the enrichment score of each sample in a specific gene set, which is suitable for discovering continuous differences in gene set activity among samples. To evaluate the immunological characteristics across all samples, we used the "GSVA" R package with the single-sample gene set enrichment analysis (ssGSEA) technique.

Animal Models and Experimental Procedures

Male C57BL/6 mice (6~8 weeks, average weight 18~22 grams) were purchased from Beijing Huafukang Technology Co. (China) and housed in specific pathogen-free room with free access to food and water. After one week of acclimation period, mice were anesthetized by isoflurane inhalation and secured in the supine position. A micro-sprayer tip was inserted into the trachea through the glottis, and 50 μL of bleomycin (2.5 mg/kg, prepared in sterile PBS) was aerosolized evenly to the lungs to build a pulmonary fibrosis model. Mice in the control group were intratracheally atomized equal volume of PBS solutions. After three weeks, all mice were anesthetized with 0.25% pentobarbital sodium (50 mg/kg, intraperitoneal injection) and sacrificed by cervical dislocation, and lung tissues were collected, with the left side embedded in paraffin for histopathology and the right side stored at −80°C for further analysis. The study was carried out in compliance with the ARRIVE guidelines. All animal experiments were strictly performed in accordance with the NIH Guide for the Care and Use of Laboratory Animals and approved by the Committee on the Ethics of Animal Experiments of West China Hospital, Sichuan University (20230922001).

Micro-Computed Tomography (Micro-CT)

Chest micro-CT was performed for mice under isoflurane anesthesia using a Quantum GX micro-CT scanner (PerkinElmer, Inc., Waltham, MA) on the day before lung sample collections. The parameters of X-ray tube were 90 KVp and 160 μA, and projection radiographs were obtained during the entire 360° gantry rotation, which took approximately 4.5 minutes for each mouse.

Histopathological and Immunohistochemical (IHC) Staining

Left lung samples were formalin-fixed, paraffin-embedded, and sectioned at 6 μm for Hematoxylin-eosin (H&E) staining, Masson staining, and Sirius red staining, and the extent of lung tissue damage and fibrosis was assessed. For IHC staining, the paraffin sections were dewaxed and rehydrated, and the microwave antigen retrieval was conducted with the citrate antigen repairing solution (1X). Then endogenous peroxidases were removed with 3% hydrogen peroxide, and sections were blocked with 5% goat serum for 20 minutes and incubated with the primary antibodies overnight at 4°C. Primary antibodies against IGF1, SMAD7, and GPX3 were purchased from ABclonal (China), the primary antibody against GADD45β was purchased from Invitrogen (USA), and the primary antibody against TIMP3 was purchased from Zenbio (China). The biotin labelled secondary antibody was applied to sections at the following day and incubated at room temperature for one hour. Finally, the color reaction was performed using the freshly prepared diaminobenzidine (DAB) solution and cell nuclei were slightly stained with hematoxylin. All specimens were scanned using the OLYMPUS VS200 full slide scanning system and digital pictures were observed and photographed by the CaseViewer 2.4.

Quantitative Real-Time PCR (qRT-PCR)

Total RNA from right upper lung tissues were extracted using the RNeasy Mini Kit (QIAGEN, Germany), and RNA concentrations were quantified by NanoDrop 2000 Spectrophotometer. RNA reverse transcription was performed using the PrimeScript^{TM} FAST RT Reagent Kit (Takara, Japan) according to the manufacturer's instructions. Target genes of IGF1, SMAD7, GPX3, GADD45β, and TIMP3 were obtained from Beijing Tsingke Biotech Co., Ltd. (China) and amplified using the FastStart Essential DNA Green Master (Roche, Switzerland) and examined by quantitative real-time PCR. β-actin was set as an internal reference and relative gene expression levels were calculated with the equation $2^{-\Delta\Delta ct}$. The primer pair sequences of mice were listed in Table 1.

Processing of Single-Cell RNA Sequencing (scRNA-Seq) Data

We accessed publicly available scRNA-seq data from the GEO database (GSE122960) consisting of 4 IPF and 8 healthy lung tissue samples. The data were analyzed using the "Seurat" and "harmony" packages in R. To ensure high-quality data, cells with a mitochondrial gene percentage higher than 15%, ribosomal gene percentage higher than 3%, erythrocyte gene percentage less than 0.1%, cell counts less than three, or cells expressing more than 5,000 genes were excluded. The gene expression of the included cells was normalized using the "NormalizeData" function in Seurat. The PCA was then performed to extract the top 15 principal components based on the top 2000 highly variable genes, identified using the "FindVariableFeatures" function. Unsupervised clustering of cell subpopulations was conducted using the "FindNeighbors", "FindClusters" (resolution = 0.5), and "RunUMAP" functions. The "SingleR" package was used to annotate cell types. Gene expression levels across different cell types were visualized using UMAP plots, and heatmaps were generated to show the proportion and expression of hub genes (GPX3, IGF1, SMAD7, GADD45β, and TIMP3) across cell types.

Statistical Analysis

R version 4.3.3 was used for bioinformatics data analyses. Results were displayed as mean ± standard deviation (SD), and the Student's *t*-test was used for comparison between two groups. GraphPad Prism 9.5.1 software (USA) was used for statistical analyses. $P < 0.05$ was considered statistically significant.

Results

Identification of DEGs and PAN-DEGs Between IPF and Normal Lung Tissues

Initially, an integrated dataset comprising 373 IPF and 158 control lung tissue samples was obtained from the GEO database, and batch effects were eliminated to generate a consolidated gene expression profile (Figure 2A and B).

Table 1 The Primer Sequences for qRT-PCR

Gene	Sequences (5' - 3')
Igf1-F	TGTCGTCTTCACACCTCTTCTAC
Igf1-R	ACATCTCCAGTCTCCTCAGATCA
Gadd45β-F	GGCCAAACTGATGAATGTGGAC
Gadd45β-R	CTGGATCAGGGTGAAGTGAATCT
Gpx3-F	TGTGCCTAATTTCCAGCTCTTTG
Gpx3-R	CAGCGGATGTCATGGATCTTCAT
Timp3-F	GGCCTCAATTACCGCTACCA
Timp3-R	ATGCAGGCGTAGTGTTTGGA
Smad7-F	CCCTCCTCCTTACTCCAGATACC
Smad7-R	GAGGGCTCTTGGACACAGTAGA
β-actin-F	CCACCATGTACCCAGGCATT
β-actin-R	CAGCTCAGTAACAGTCCGCC

Abbreviations: qRT-PCR, quantitative real-time polymerase chain reaction; Igf1, insulin-like growth factor 1; Gadd45β, growth arrest and DNA damage-inducible 45-beta; Gpx3, glutathione peroxidase 3; Timp3, tissue inhibitor of metalloproteinase 3; Smad7, mothers against decapentaplegic homolog 7.

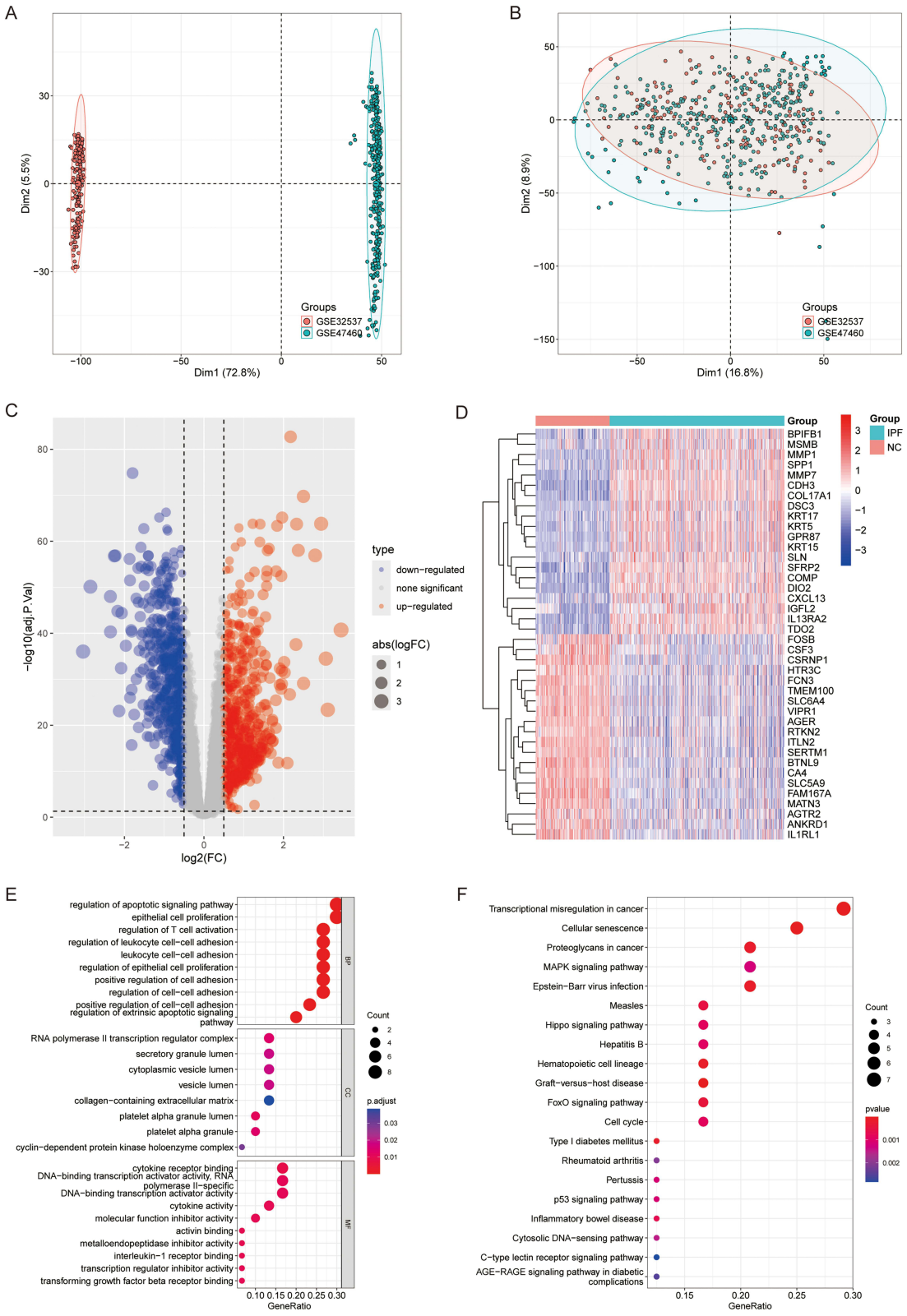

Figure 2 Comparative gene expression and functional annotation analysis in datasets GSE32537 and GSE47460 related to Idiopathic Pulmonary Fibrosis (IPF) and Normal Control (NC) samples. (**A**) PCA plot showing the separation between the two datasets. (**B**) PLS-DA plot depicting the discrimination between the datasets. (**C**) Volcano plot of differentially expressed genes, with up-regulated genes in red, down-regulated genes in blue, and non-significant genes in grey. (**D**) Heatmap of top differentially expressed genes between IPF and NC samples, with higher expression in red and lower in blue. (**E**) GO enrichment analysis bar plot for biological processes, with dot size representing gene count and color indicating adjusted p-value. (**F**) KEGG pathway enrichment analysis bar plot, with dot size representing gene ratio and color indicating p-value.

https://doi.org/10.2147/JIR.S505229

Overall, 663 up-regulated and 667 down-regulated DEGs were identified and visualized in a volcano plot (Figure 2C). Among these, BPIFB1, MSMB, MMP1, SPP1, and MMP7 were the top five up-regulated genes in the lung tissues of IPF patients, whereas IL1RL1, ANKRO1, AGTR2, MATN3, and FAM167A exhibited the most significantly down-regulated expressions (Figure 2D). GO analysis revealed that the DEGs were primarily associated with apoptotic signaling, cell proliferation, and adhesion processes, with molecular functions enriched in cytokine activity, receptor binding, and DNA-binding transcription activator activity (Figure 2E). The KEGG analysis identified significant associations with cellular senescence, the cell cycle, and critical signaling pathways including MAPK, Hippo, FoxO, and p53 (Figure 2F).

The intersection of PANoptosis-related genes with DEGs in IPF revealed 30 overlapping genes, including 12 up-regulated and 18 down-regulated genes (Figure 3A and B). A heat map illustrated the expression profiles of these PAN-DEGs in IPF (Figure 3C). Furthermore, the WGCNA analysis identified 25 co-expression modules, with their relationships to specific characteristics depicted in Figure 3D, E, and Supplementary Figure 1.

PPI Network Construction and Identification of Hub PANoptosis-Related Gene Signatures

To predict potential functions and interactions of PANoptosis-related gene sets in IPF, a PPI network was conducted using the online tool GeneMANIA (Figure 4A). Hub genes associated with PANoptosis were identified via machine learning, specifically employing LASSO regression, support vector machine (SVM), and random forest algorithms to isolate key genes (Figure 4B–D). This analysis resulted in the establishment of a five-gene PANoptosis-related signature, consisting of GPX3, TIMP3, SMAD7, IGF1, and GADD45β.

Validation of Hub PANoptosis-Related Gene Expression and Their Diagnostic Performance

The expression levels of hub PANoptosis-related genes from internal datasets are presented in Figure 5A. In IPF lung tissues, IGF1 was found to be up-regulated, whereas GPX3, TIMP3, SMAD7, and GADD45β were down-regulated. Subsequent to our initial findings, we conducted further validation of the gene expressions using an external dataset from GEO (GSE110147), confirming that all five genes retained statistical significance (Figure 5B). Gene Set Variation Analysis (GSVA) indicated that these genes were significantly linked to several pathways, including TGF-β, Wnt/β-catenin, PI3K/Akt/mTOR, NF-κB, and p53. This association suggests their involvement in processes such as epithelial-mesenchymal transition, cellular senescence, inflammation, oxidative stress, glycolysis, and fatty acid metabolism (Figure 5C). A Circos plot illustrated the interrelationships among the PANoptosis-related genes, notably identifying a negative correlation between IGF1 and the other four genes (Figure 5D). Furthermore, ROC curves demonstrated robust diagnostic capabilities, with each gene achieving an AUC exceeding 0.80. As expected, the combined genes attained the highest AUC of 0.945 (Figure 5E).

Immune Cell Fraction Analysis and Correlation with Hub Gene Expression

Figure 6A depicted the proportions of various immune cell types in IPF and NC samples, revealing significant differences between the groups. Violin plots further elucidated the distribution of these immune cells, emphasizing alterations in cell types such as naive B cells, memory B cells, plasma cells, T cells, monocytes, macrophages, dendritic cells, eosinophils, and neutrophils. The heat map analysis presented in Figure 6B illustrates the correlation between the expression levels of hub PANoptosis-related genes (IGF1, GADD45β, TIMP3, SMAD7, and GPX3) and the proportions of various immune cell types. These correlations imply potential interactions between PANoptosis-related genes and the immune microenvironment in IPF.

Validation of PANoptosis-Related Gene Signature in a Bleomycin-Induced Pulmonary Fibrosis Model

To further substantiate the expression levels of the five PANoptosis-related candidate genes identified through bioinformatic analyses, we established a bleomycin-induced murine model of pulmonary fibrosis. This was initially confirmed

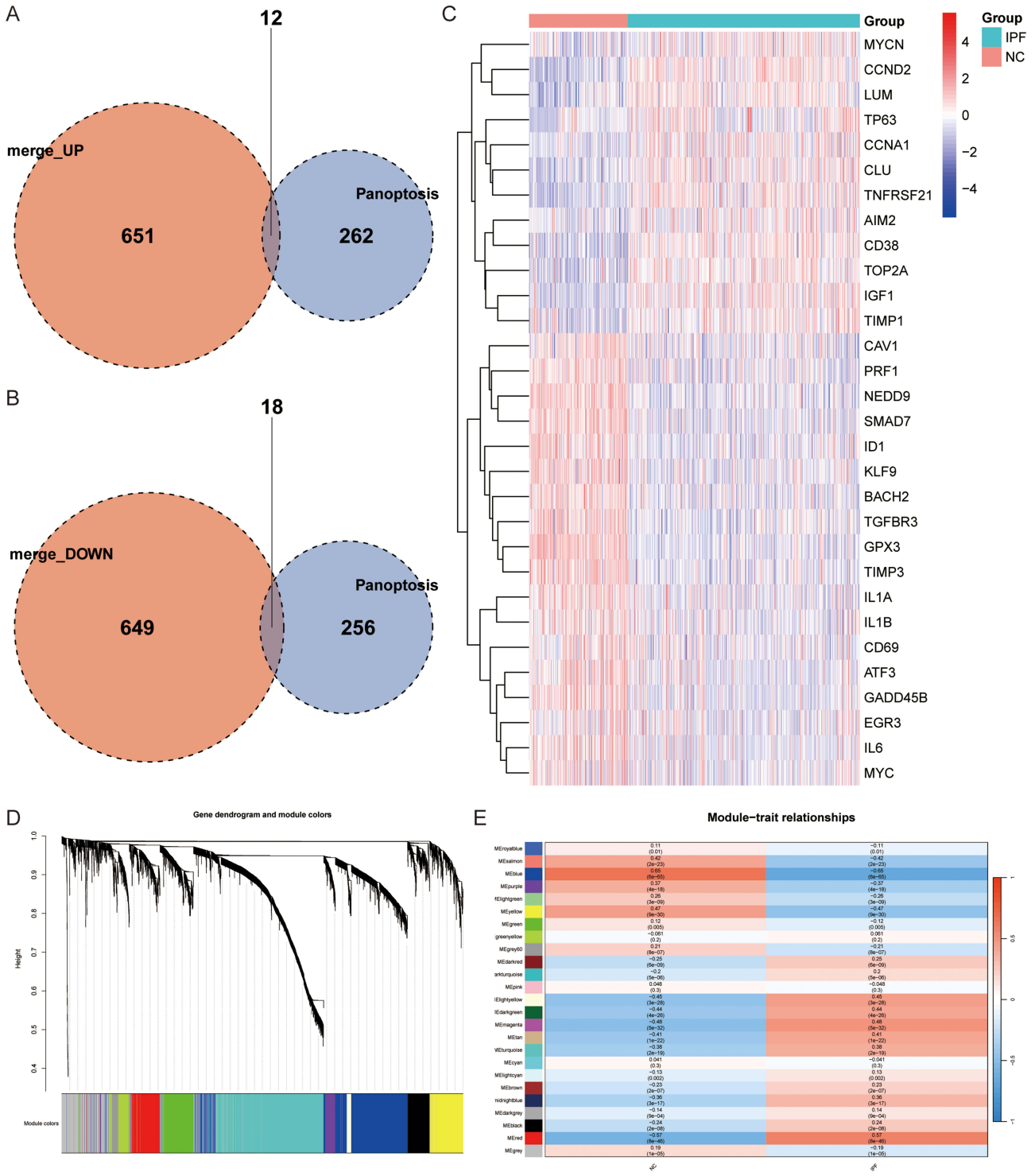

Figure 3 Analysis of differentially expressed genes and gene co-expression modules in IPF and NC samples. (**A** and **B**) Venn diagrams showing the overlap of up-regulated and down-regulated genes between merged datasets and panoptosis-related genes. (**C**) Heatmap of selected differentially expressed genes in IPF and NC samples, with higher expression in red and lower in blue. (**D**) Gene dendrogram and module colors from weighted gene co-expression network analysis. (**E**) Heatmap of module-trait relationships, with colors representing the correlation between module eigengenes and traits, and values indicating correlation coefficients.

using micro-CT technology and lung histological examination to ensure the successful development of the murine pulmonary fibrosis model. As shown in Figure 7A, the model group exhibited reduced lung transmittance on chest CT, characterized by an increased percentage of non-aerated parenchyma and thickening of bronchial walls and interlobar fissures. H&E staining revealed the disappearance of normal alveolar structures in fibrotic lung tissues, replaced by

https://doi.org/10.2147/JIR.S505229

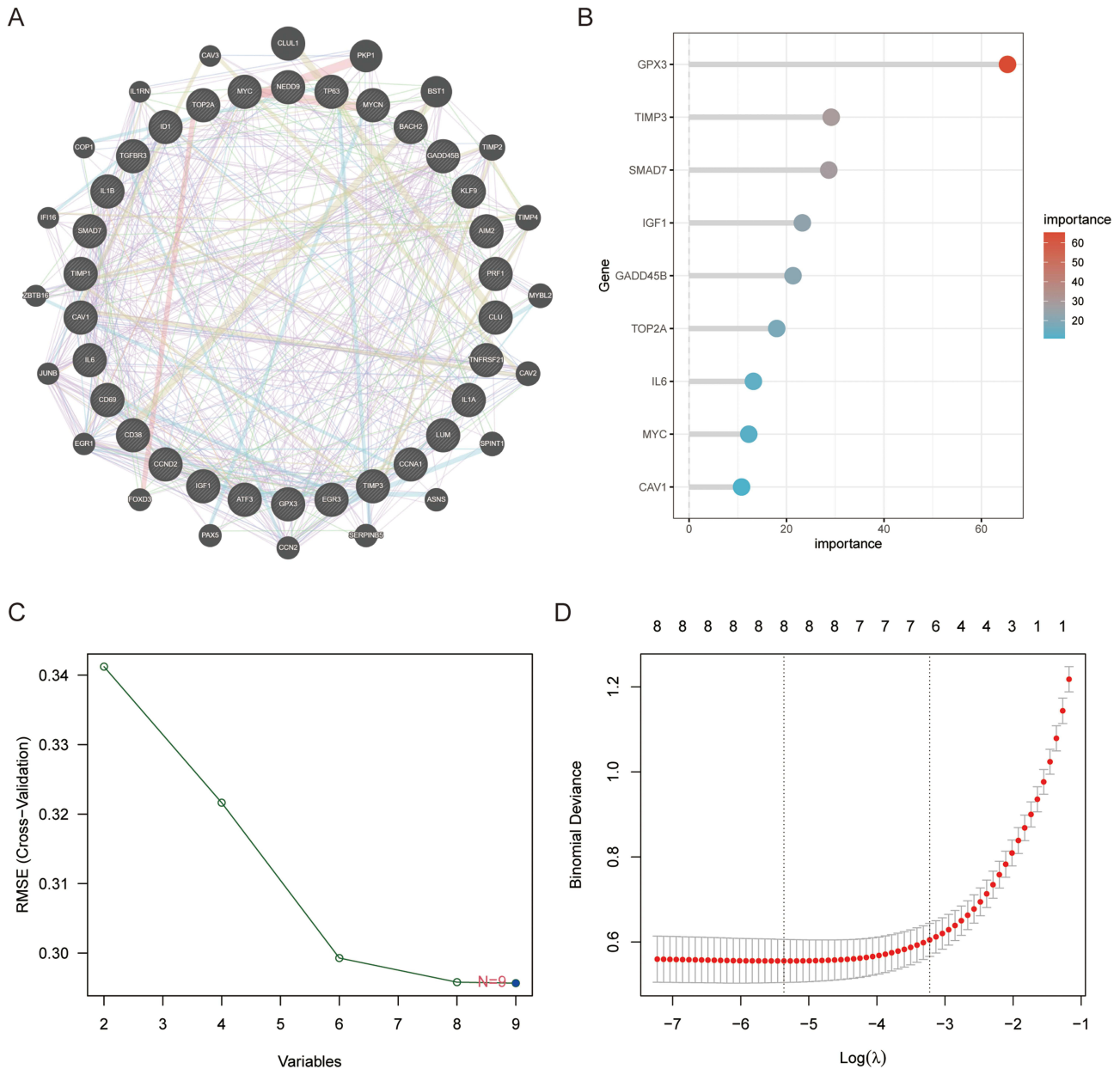

Figure 4 Protein-protein interaction (PPI) network and hub gene selection for PANoptosis-related genes. (**A**) PPI network generated using GeneMANIA, showing interactions between PANoptosis-related proteins. (**B**) Variable importance plot highlighting the top hub gene. (**C**) Cross-validation RMSE for selecting the optimal number of variables. (**D**) Binomial deviance for the logistic regression model with different λ values.

inflammatory cell infiltration and the proliferation of tissue cells within the alveolar cavity. Furthermore, Masson's trichrome and Sirius red staining confirmed the excessive deposition of collagen fibers in fibrotic lungs (Figure 7B). In comparison to normal controls, the signature genes were significantly expressed in bleomycin-induced murine pulmonary fibrosis samples aligning with findings from external validation (Figure 7C and D).

Differential Cell Type Distribution and Hub Gene Expression in IPF Lung Tissues Revealed by ScRNA-Seq

The analysis of lung tissue samples from patients with IPF and healthy controls revealed marked differences in cell type distributions and gene expression profiles. Uniform Manifold Approximation and Projection (UMAP) plots illustrated distinct clustering of various cell types, including epithelial cells, T cells, endothelial cells, macrophages, mast cells,

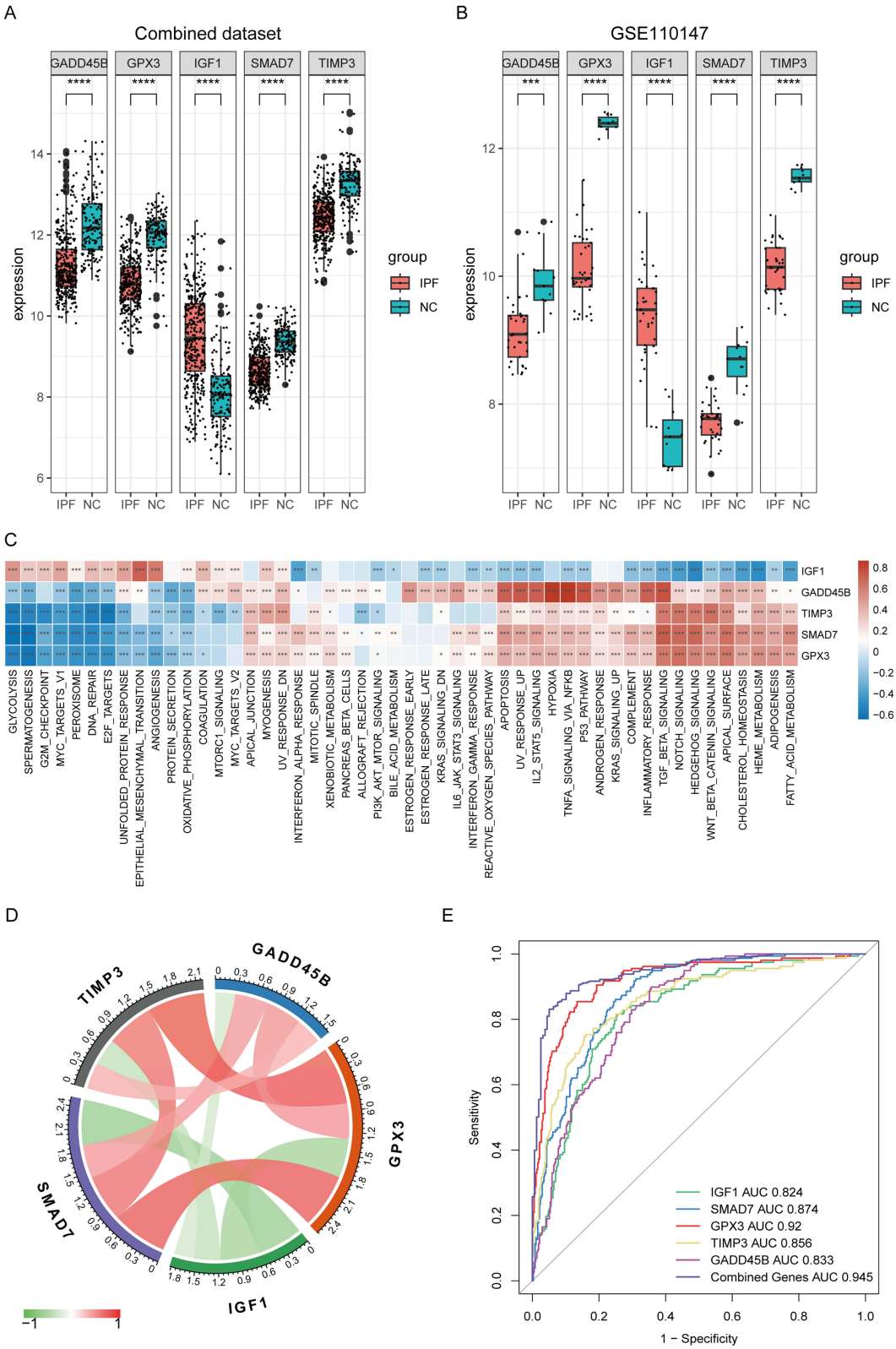

Figure 5 Gene expression analysis and diagnostic performance in Idiopathic Pulmonary Fibrosis (IPF) and Normal Control (NC) samples. (**A**) Box plots showing the expression levels of hub genes in the combined dataset for IPF and NC samples. (**B**) Box plots displaying the expression levels of the same hub genes in the GSE110147 dataset. (**C**) Heatmap of gene set enrichment analysis results, illustrating the association between hub genes and various biological pathways, with color intensity representing the enrichment score. (**D**) Circos plot depicting the correlation between hub genes, with the strength of correlation indicated by the thickness of connecting lines. (**E**) Receiver Operating Characteristic curves for hub genes, showing their diagnostic performance with the Area Under the Curve values for hub genes. *P < 0.05, **P < 0.01, ***P < 0.001, and ****P < 0.0001.

https://doi.org/10.2147/JIR.S505229

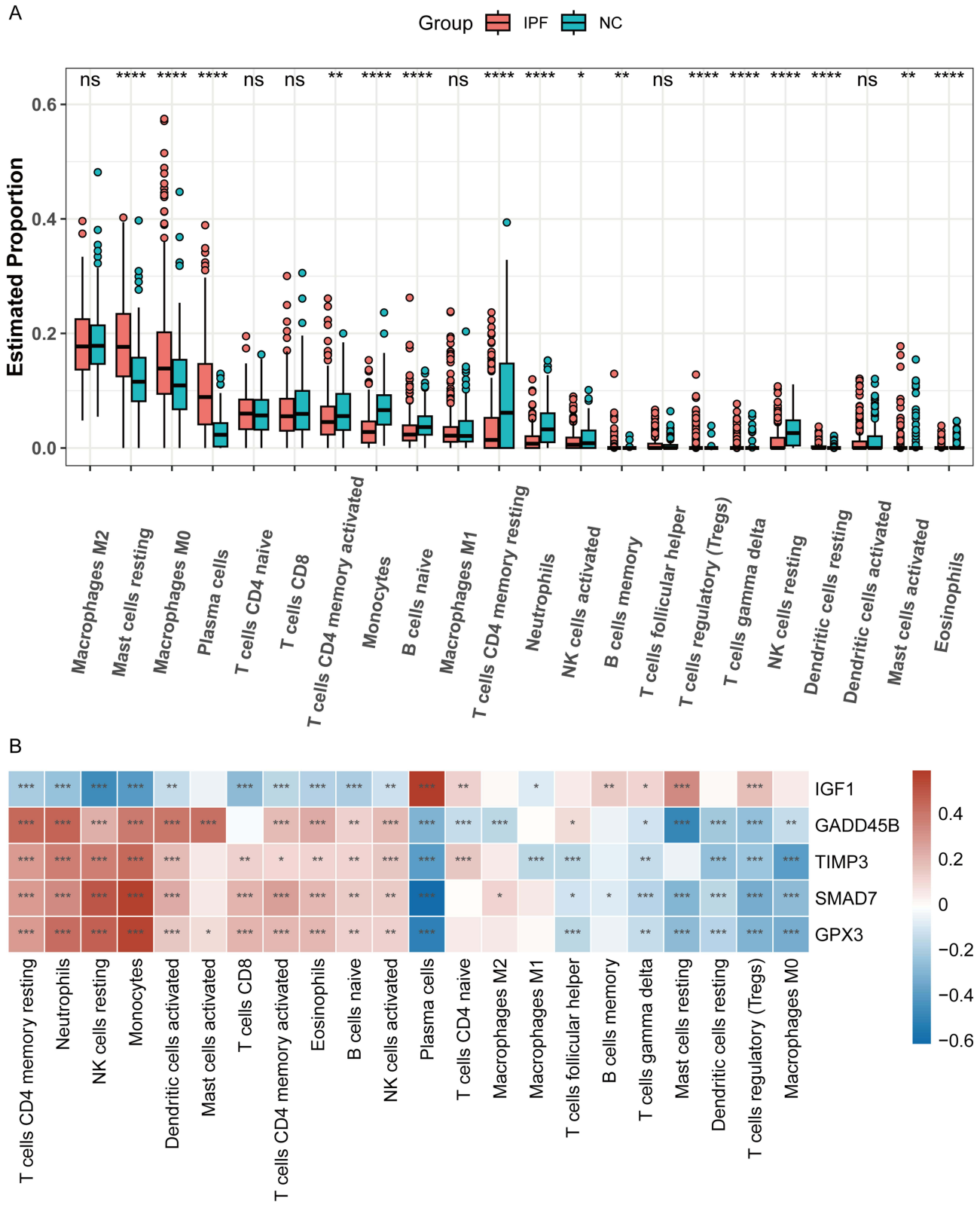

Figure 6 Immune cell fraction analysis and correlation with hub gene expression in IPF and NC samples. (**A**) Violin plots showing the fractions of different immune cell types in IPF and NC samples. Significant differences between groups are indicated. (**B**) Heatmap illustrating the correlation between hub gene expression and the fractions of various immune cell types, with color intensity representing the correlation coefficient. *P < 0.05, **P < 0.01, ***P < 0.001, and ****P < 0.0001.

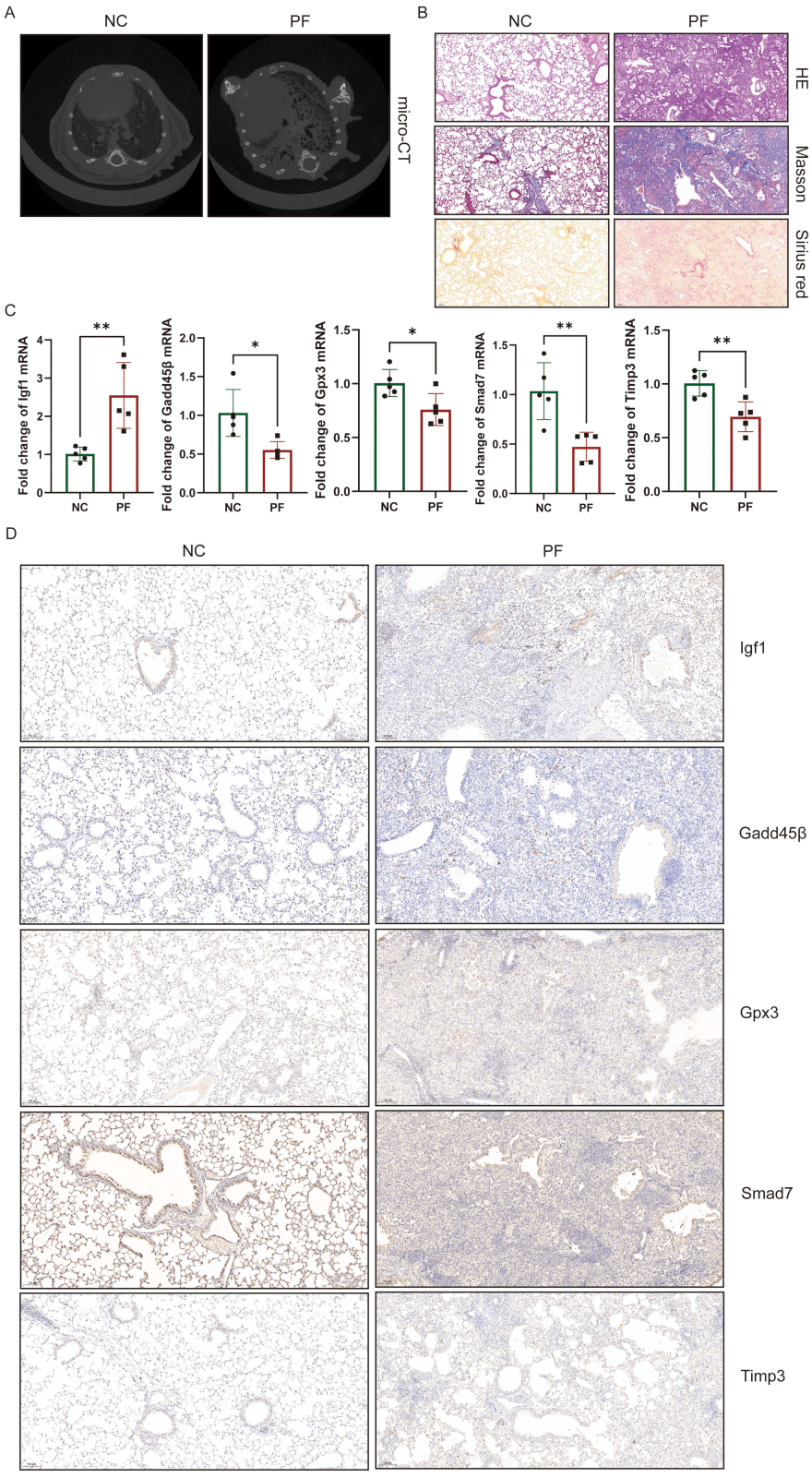

Figure 7 Construction of bleomycin-induced murine pulmonary fibrosis and gene expression analyses in vivo. (**A**) micro-CT showing radiological changes in Pulmonary Fibrosis (PF) and Normal Control (NC) lungs. (**B**) H&E, Masson, and Sirius red staining showing the pathological changes in PF and NC left lung samples. (**C**) qRT-PCR validating the expression levels of hub genes in PF and NC samples (n = 5 per group). (**D**) Immunohistochemical (IHC) staining validating the expression levels of hub genes in PF and NC samples (n = 3 per group). *P < 0.05, and **P < 0.01.

https://doi.org/10.2147/JIR.S505229

monocytes, plasma cells, fibroblasts, and B cells, with a notably higher proportion of fibroblasts observed in IPF samples (Figure 8A). The heat map of cluster scores indicated variations in relative expression levels among different cell clusters, with elevated scores in specific clusters suggesting increased activity or abundance of certain cell types in IPF (Figure 8B). Heat maps depicting the proportion and expression levels of hub genes across various cell types showed distinct patterns. For instance, GPX3 and IGF1 exhibited significantly increased expression in fibroblasts and macrophages in IPF samples compared to controls, illustrating their potential involvement in fibrosis and inflammatory pathways, respectively (Figure 8C and D). UMAP plots of individual hub genes further delineate specific expression patterns within different cell populations. GPX3 was predominantly upregulated in fibroblasts, IGF1 in both fibroblasts and macrophages, SMAD7 in epithelial cells, GADD45β in T cells, and TIMP3 in endothelial cells. These findings

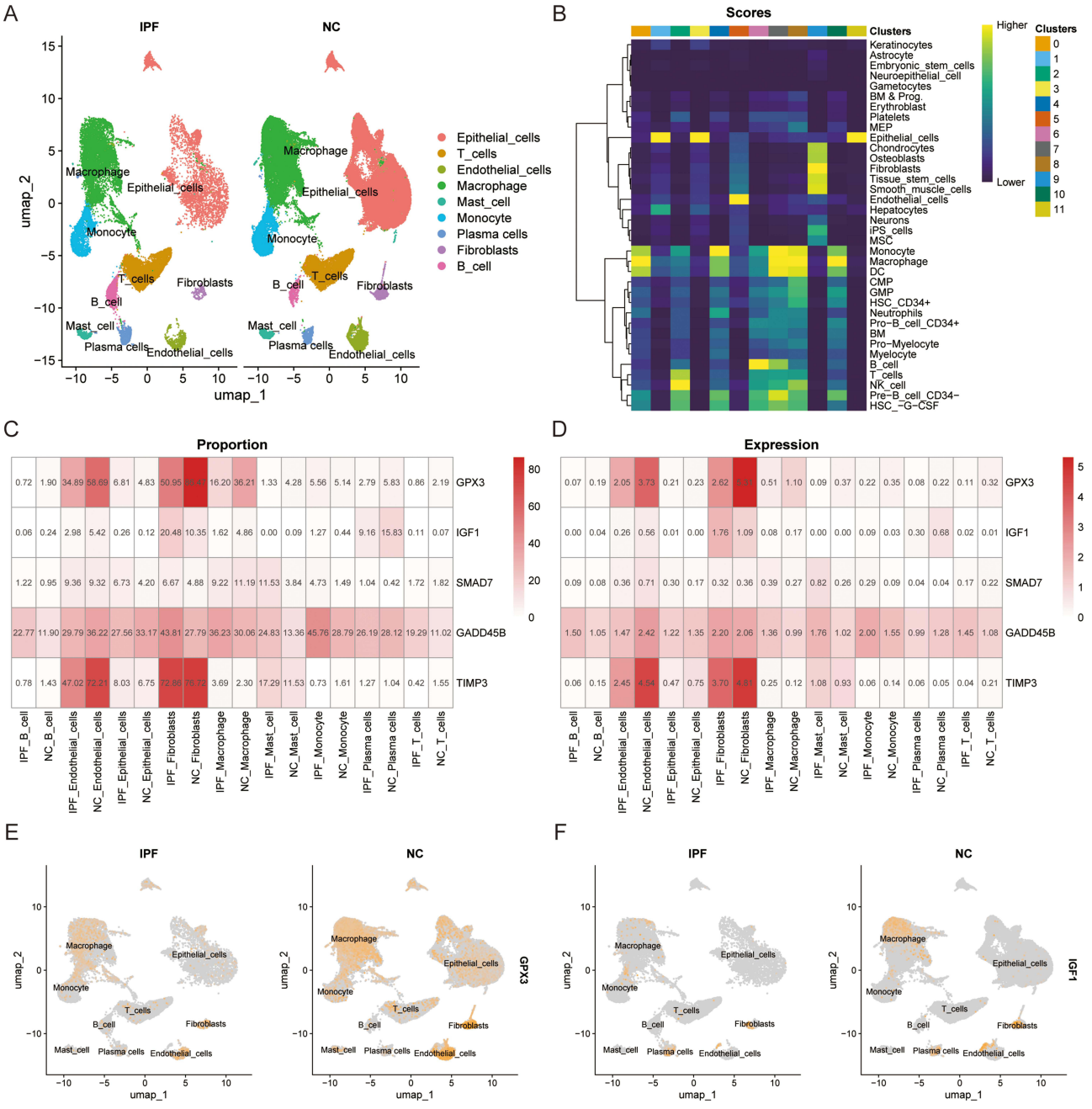

Figure 8 Continued.

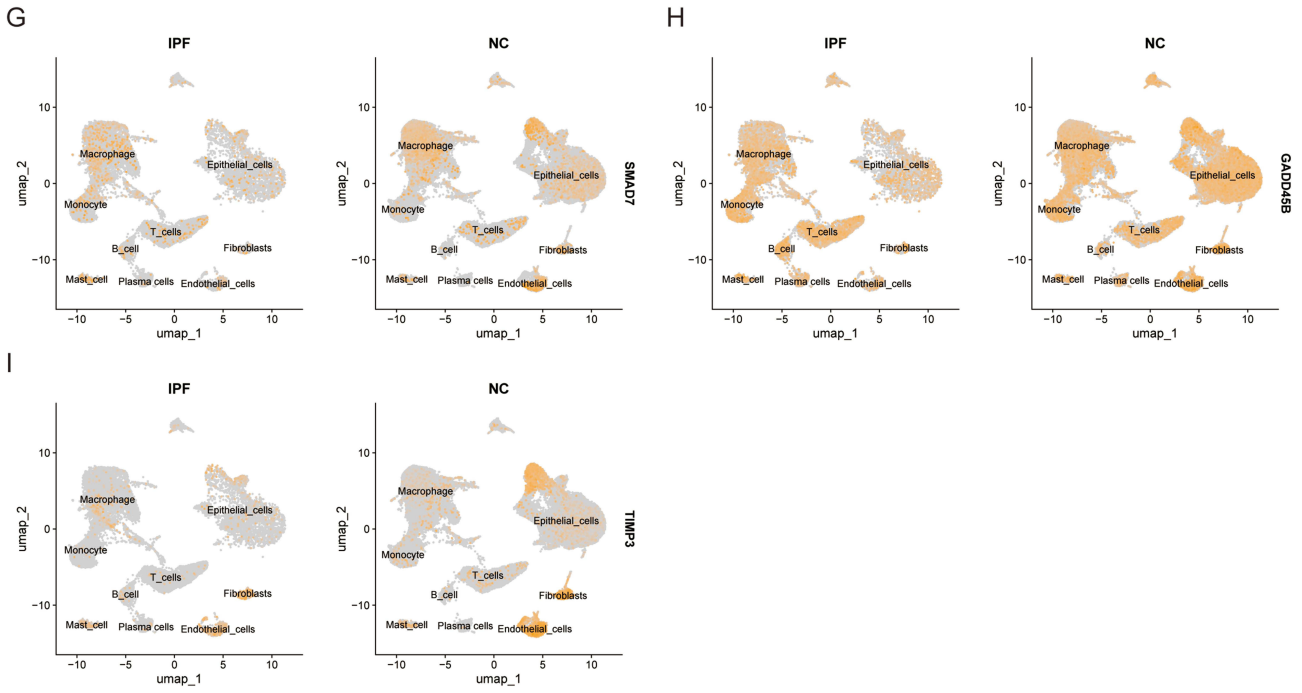

Figure 8 Cell type distributions and hub gene expression in Idiopathic Pulmonary Fibrosis (IPF) and Normal Control (NC) samples. (**A**) UMAP plots showing the distribution of various cell types in IPF and NC samples. (**B**) Heatmap of cell cluster scores in IPF and NC samples, with clusters listed on the right and colors representing score levels; higher scores are indicated by brighter colors. (**C**) Heatmap depicting the proportion of cells expressing hub genes across different cell types in IPF and NC samples, with color intensity representing the proportion; darker red indicates higher proportions. (**D**) Heatmap illustrating the expression levels of hub genes in various cell types from IPF and NC samples, with color intensity indicating expression levels; darker red signifies higher expression. (**E–I**) UMAP plots showing the expression of individual hub genes in cell populations from IPF and NC samples. Each plot highlights cells expressing a specific gene, with positive cells marked in Orange and non-expressing cells in grey.

indicate the diverse functions these genes serve across various cell types and underscore notable differences between IPF and control samples (Figure 8E–I).

Discussion

Interstitial pneumonias encompass a broad category of diseases with diverse etiologies and heterogeneous histopathological and radiological features.[20] Typically, pulmonary fibrosis manifests in the advanced stages, signifying an irreversible and fatal progression. In fibrosis arising from various etiologies, IPF remains a prevalent form, with recent estimates of global incidence ranging from 0.09 to 1.30 per 10,000 population and prevalence between 0.33 and 4.51 per 10,000 population.[21] The prognosis for IPF is notably poor, with a median expected life span of 3–5 years from diagnosis.[22] Despite advancements in anti-fibrotic therapies designed to decelerate the deterioration of pulmonary function and disease progression, a definitive cure for IPF remains elusive. Risk factors for IPF encompass both genetic predispositions and environmental exposures, including age, tobacco use, viral infections, and occupational exposure to certain particles or chemicals.[23] Apoptosis, pyroptosis, and necroptosis have been implicated in the pathogenesis of IPF, playing critical roles in tissue remodeling; however, targeting these pathways individually may prove insufficient.[8,24] Hence, there is an increasing interest in developing a comprehensive therapeutic approach for IPF by targeting distinct cell death pathways.

PANoptosis is a newly proposed inflammatory cell death modality representing a complex interplay among apoptosis, pyroptosis and necroptosis.[25] This novel cell death pathway is characterized by the simultaneous activation of these three distinct processes, which are traditionally considered separate. The concept of PANoptosis has emerged from the recognition of the extensive crosstalk and mechanistic overlaps among these pathways, leading to the formation of a multiprotein complex known as the PANoptosome. This complex integrates components from each pathway, facilitating a coordinated cell death response that can bypass pathogen-mediated inhibition of individual pathways.[26] Accumulating evidence demonstrate that PANoptosis is intricately involved in cell homeostasis and occurs under vast and multifarious stimuli.[27] In cancer, for instance, PANoptosis has been associated with the tumor immune microenvironment, offering

https://doi.org/10.2147/JIR.S505229

potential therapeutic applications. The ability of PANoptosis to modulate immune responses and influence tumor progression makes it a promising target for cancer therapy.[28] Furthermore, PANoptosis plays a crucial role in autoimmune diseases, where it contributes to systemic chronic inflammation and abnormal immune responses. The dual role of PANoptosis in both promoting and regulating inflammation underscores its complexity and potential as a therapeutic target in autoimmune conditions.[29]

In addition to cancer and autoimmune diseases, PANoptosis is implicated in infectious diseases, where it serves as a defense mechanism against pathogens. The activation of PANoptosis during infections, such as those caused by influenza virus and bacterial pathogens, demonstrates its role in host defense by eliminating infected cells and preventing pathogen spread.[30] The ability of PANoptosis to integrate signals from various cell death pathways and respond to diverse stimuli makes it a critical component of the innate immune response, with implications for the development of novel therapeutic strategies targeting inflammatory and infectious diseases.[31] The involvement of PANoptosis in various diseases highlights its significant pathophysiological relevance.

Through bioinformatics analysis, we identified five potential PANoptosis-related signature genes associated with the pathogenesis of idiopathic pulmonary fibrosis: IGF1, GPX3, GADD45β, SMAD7, and TIMP3. Besides, the expression patterns of these significant candidate genes were validated in a murine model of bleomycin-induced pulmonary fibrosis. Our results showed that the differences in expression levels of all five genes remained statistically significant. Subsequently, we examined the molecular functions and cellular localization of these genes within the lungs, discovering that the PANoptosis-related genes exhibited a positive correlation with various pro-fibrotic processes including epithelial-mesenchymal transition, cellular senescence, inflammation, and oxidative stress. Utilizing single-cell sequencing techniques, we also projected the expression and distribution of these genes in pulmonary cells.

The involvement of various molecular pathways, including those mediated by IGF1 and SMAD7, has been a focus of research in understanding IPF's pathogenesis and progression. IGF1 signaling has been implicated in the disease's pathogenesis due to its role in cellular proliferation and differentiation.[32,33] SMAD7 serves as a negative feedback regulator of the TGF-β signaling pathway, which is also crucial in fibrosis development.[34] Besides, TIMP3 was found remarkably expressed in IPF tissues and localized to fibroblastic foci and extracellular matrix (ECM), and TGF-β1 could induce strong up-regulation of TIMP3 at the mRNA and protein levels, suggesting it as an important mediator in lung fibrogenesis.[35] By contrast, studies specifically focusing on the roles of GPX3 and GADD45β in pulmonary fibrosis are limited. GPX3, an extracellular antioxidant enzyme, has been studied in the context of cancer and metabolic syndrome, where it plays a role in modulating oxidative stress and cellular redox balance.[36,37] GADD45β is known for its involvement in cellular stress responses, including DNA repair, apoptosis, and cell cycle regulation. It has also been implicated in various inflammatory and cancer-related processes.[38,39] While these studies provide insights into the functions of GPX3 and GADD45β in other diseases, their specific contributions to IPF pathogenesis are not well-documented. A previous study accessed the regulation and distribution of GPX3 in murine and human pulmonary fibrosis and found that GPX3 localized to ECM and was upregulated in lung homogenates from IPF patients, revealing an effect of GPX3 on IPF.[40] In short, although these molecules are related to the fibrotic process, whether they regulate fibrosis through PANoptosis pathways require further investigation. Understanding these roles could provide new insights into molecular mechanisms of IPF and identify potential therapeutic targets for this debilitating disease.

It is important to acknowledge several limitations of this study. First, the PANoptosis-related gene set was derived from previous studies, and our conclusions are based solely on the current dataset. Therefore, the functional mechanisms and interactions of identified genes in relation to PANoptosis remain uncertain and warrant further experimental investigation. Second, the selection of current PANoptosis signature genes related to IPF was conducted using public databases and comprehensive bioinformatic analyses. The heterogeneity among studies may affect the reliability of results. To address this issue, we chose two datasets with the largest sample sizes to identify PANoptosis-related genes and then validated their expressions at both transcriptional and translational levels. Third, due to the challenges in obtaining lung samples from IPF patients, we utilized murine fibrotic lung tissues as a substitute, which may not fully represent gene expression changes in IPF patients. In general, further research should include gene knockout/overexpression experiments, protein interaction network analyses, and clinical studies to elucidate the functions of PANoptosis-related genes.

In conclusion, this study identified several novel targets potentially involved in PANoptosis and IPF processes, which could serve as potential diagnostic biomarkers for IPF. More to the point, our findings demonstrated that these genes are correlated with various immune cells and provided potential distribution information within pulmonary cells. More studies are further required to elucidate the biological functions and mechanisms of these genes in the pathogenesis of IPF.

Data Sharing Statement

The datasets presented in this study can be found in online repositories, and names of these repositories and accession numbers are shown in the article material. Other data is available from the corresponding author upon reasonable request.

Ethics Approval

The animal experiment was approved by the Committee on the Ethics of Animal Experiments of West China Hospital, Sichuan University (20230922001). All experimental methods were strictly performed in accordance with the NIH Guide for the Care and Use of Laboratory Animals. The human data used in this study were all from publicly available databases (GEO). According to Article 32, item 1 and 2 of the Measures for Ethical Review of Life Science and Medical Research Involving Human Beings dated February 18, 2023, China, secondary analysis based on publicly anonymous data does not require additional ethical review.

Acknowledgments

We acknowledge the GEO database for providing platforms and researchers for sharing their meaningful data sets.

Author Contributions

All authors made a significant contribution to the work reported, whether that is in the conception, study design, execution, acquisition of data, analysis and interpretation, or in all these areas; took part in drafting, revising or critically reviewing the article; gave final approval of the version to be published; have agreed on the journal to which the article has been submitted; and agree to be accountable for all aspects of the work.

Funding

This study was supported by Sichuan Science and Technology Program (2024NSFSC1529), and National Clinical Research Center for Geriatrics, West China Hospital, Sichuan University, China (Z2024LC005).

Disclosure

All authors declare that they have no conflicts of interest in this work.

References

1. Podolanczuk AJ, Thomson CC, Remy-Jardin M, et al. Idiopathic pulmonary fibrosis: state of the art for 2023. *Eur Respir J*. 2023;61(4).
2. Khor YH, Ng Y, Barnes H, Goh NSL, McDonald CF, Holland AE. Prognosis of idiopathic pulmonary fibrosis without anti-fibrotic therapy: a systematic review. *Eur Respir Rev*. 2020;29(157).
3. Yuan J, Ofengeim D. A guide to cell death pathways. *Nat Rev mol Cell Biol*. 2024;25(5):379–395. doi:10.1038/s41580-023-00689-6
4. Kari S, Subramanian K, Altomonte IA, Murugesan A, Yli-Harja O, Kandhavelu M. Programmed cell death detection methods: a systematic review and a categorical comparison. *Apoptosis*. 2022;27(7–8):482–508. doi:10.1007/s10495-022-01735-y
5. Ketelut-Carneiro N, Fitzgerald KA. Apoptosis, pyroptosis, and necroptosis-oh my! The many ways a cell can die. *J mol Biol*. 2022;434(4):167378. doi:10.1016/j.jmb.2021.167378
6. Waisberg DR, Barbas-Filho JV, Parra ER, et al. Abnormal expression of telomerase/apoptosis limits type II alveolar epithelial cell replication in the early remodeling of usual interstitial pneumonia/idiopathic pulmonary fibrosis. *Hum Pathol*. 2010;41(3):385–391. doi:10.1016/j.humpath.2009.08.019
7. Lee JM, Yoshida M, Kim MS, et al. Involvement of alveolar epithelial cell necroptosis in idiopathic pulmonary fibrosis pathogenesis. *Am J Respir Cell mol Biol*. 2018;59(2):215–224. doi:10.1165/rcmb.2017-0034OC
8. Liu X, Zhang L, Zhu B, et al. Role of GSDM family members in airway epithelial cells of lung diseases: a systematic and comprehensive transcriptomic analysis. *Cell Biol Toxicol*. 2023;39(6):2743–2760. doi:10.1007/s10565-023-09799-5
9. Chen W, Gullett JM, Tweedell RE, Kanneganti TD. Innate immune inflammatory cell death: PANoptosis and PANoptosomes in host defense and disease. *Eur J Immunol*. 2023;53(11):e2250235. doi:10.1002/eji.202250235

10. He YQ, Deng JL, Zhou CC, et al. Ursodeoxycholic acid alleviates sepsis-induced lung injury by blocking PANoptosis via STING pathway. *Int Immunopharmacol*. 2023;125(Pt B):111161. doi:10.1016/j.intimp.2023.111161
11. Messaoud-Nacer Y, Culerier E, Rose S, et al. STING agonist diABZI induces PANoptosis and DNA mediated acute respiratory distress syndrome (ARDS). *Cell Death Dis*. 2022;13(3):269. doi:10.1038/s41419-022-04664-5
12. Liang Y, Yan Y, Liu N, Wang J, Fang C. Shengxian decoction improves lung function in rats with bleomycin-induced idiopathic pulmonary fibrosis through the inhibition of PANoptosis. *J Ethnopharmacol*. 2024;329:118153. doi:10.1016/j.jep.2024.118153
13. Moss BJ, Ryter SW, Rosas IO. Pathogenic mechanisms underlying idiopathic pulmonary fibrosis. *Annu Rev Pathol*. 2022;17:515–546. doi:10.1146/annurev-pathol-042320-030240
14. Barrett T, Wilhite SE, Ledoux P, et al. NCBI GEO: archive for functional genomics data sets–update. *Nucleic Acids Res*. 2013;41(Database issue):D991–995. doi:10.1093/nar/gks1193
15. Langfelder P, Horvath S. WGCNA: an R package for weighted correlation network analysis. *BMC Bioinf*. 2008;9(1):559. doi:10.1186/1471-2105-9-559
16. Shi X, Gao X, Liu W, et al. Construction of the panoptosis-related gene model and characterization of tumor microenvironment infiltration in hepatocellular carcinoma. *Oncol Res*. 2023;31(4):569–590. doi:10.32604/or.2023.028964
17. Franz M, Rodriguez H, Lopes C, et al. GeneMANIA update 2018. *Nucleic Acids Res*. 2018;46(W1):W60–W64. doi:10.1093/nar/gky311
18. Liaw A, Wiener M. Classification and regression by randomForest. *R News*. 2001;2:18–22.
19. Friedman J, Hastie T, Tibshirani R. Regularization paths for generalized linear models via coordinate descent. *J Stat Softw*. 2010;33(1):1–22. doi:10.18637/jss.v033.i01
20. Renzoni EA, Poletti V, Mackintosh JA. Disease pathology in fibrotic interstitial lung disease: is it all about usual interstitial pneumonia? *Lancet*. 2021;398(10309):1437–1449. doi:10.1016/S0140-6736(21)01961-9
21. Maher TM, Bendstrup E, Dron L, et al. Global incidence and prevalence of idiopathic pulmonary fibrosis. *Respir Res*. 2021;22(1):197. doi:10.1186/s12931-021-01791-z
22. Ley B, Collard HR, King TE Jr. Clinical course and prediction of survival in idiopathic pulmonary fibrosis. *Am J Respir Crit Care Med*. 2011;183(4):431–440. doi:10.1164/rccm.201006-0894CI
23. Strykowski R, Adegunsoye A. Idiopathic pulmonary fibrosis and progressive pulmonary fibrosis. *Immunol Allergy Clin North Am*. 2023;43(2):209–228. doi:10.1016/j.iac.2023.01.010
24. Sauler M, Bazan IS, Lee PJ. Cell death in the lung: the apoptosis-necroptosis axis. *Annu Rev Physiol*. 2019;81:375–402. doi:10.1146/annurev-physiol-020518-114320
25. Sun X, Yang Y, Meng X, Li J, Liu X, Liu H. PANoptosis: mechanisms, biology, and role in disease. *Immunol Rev*. 2024;321(1):246–262. doi:10.1111/imr.13279
26. Christgen S, Zheng M, Kesavardhana S, et al. Identification of the PANoptosome: a molecular platform triggering pyroptosis, apoptosis, and necroptosis (PANoptosis). *Front Cell Infect Microbiol*. 2020;10:237. doi:10.3389/fcimb.2020.00237
27. Wang Y, Kanneganti TD. From pyroptosis, apoptosis and necroptosis to PANoptosis: a mechanistic compendium of programmed cell death pathways. *Comput Struct Biotechnol J*. 2021;19:4641–4657. doi:10.1016/j.csbj.2021.07.038
28. Cai H, Lv M, Wang T. PANoptosis in cancer, the triangle of cell death. *Cancer Med*. 2023;12(24):22206–22223. doi:10.1002/cam4.6803
29. Liu K, Wang M, Li D, et al. PANoptosis in autoimmune diseases interplay between apoptosis, necrosis, and pyroptosis. *Front Immunol*. 2024;15:1502855. doi:10.3389/fimmu.2024.1502855
30. Zheng M, Kanneganti TD. The regulation of the ZBP1-NLRP3 inflammasome and its implications in pyroptosis, apoptosis, and necroptosis (PANoptosis). *Immunol Rev*. 2020;297(1):26–38. doi:10.1111/imr.12909
31. Bae H, Jang Y, Karki R, Han JH. Implications of inflammatory cell death-PANoptosis in health and disease. *Arch Pharm Res*. 2024;47(7):617–631. doi:10.1007/s12272-024-01506-0
32. Hernandez DM, Kang JH, Choudhury M, et al. IPF pathogenesis is dependent upon TGFbeta induction of IGF-1. *FASEB J*. 2020;34(4):5363–5388. doi:10.1096/fj.201901719RR
33. Sun W, Jing X, Yang X, et al. Regulation of the IGF1 signaling pathway is involved in idiopathic pulmonary fibrosis induced by alveolar epithelial cell senescence and core fucosylation. *Aging*. 2021;13(14):18852–18869. doi:10.18632/aging.203335
34. Hu HH, Chen DQ, Wang YN, et al. New insights into TGF-beta/Smad signaling in tissue fibrosis. *Chem Biol Interact*. 2018;292:76–83. doi:10.1016/j.cbi.2018.07.008
35. Garcia-Alvarez J, Ramirez R, Checa M, et al. Tissue inhibitor of metalloproteinase-3 is up-regulated by transforming growth factor-beta1 in vitro and expressed in fibroblastic foci in vivo in idiopathic pulmonary fibrosis. *Exp Lung Res*. 2006;32(5):201–214. doi:10.1080/01902140600817481
36. Worley BL, Kim YS, Mardini J, et al. GPx3 supports ovarian cancer progression by manipulating the extracellular redox environment. *Redox Biol*. 2019;25:101051. doi:10.1016/j.redox.2018.11.009
37. Baez-Duarte BG, Mendoza-Carrera F, Garcia-Zapien A, et al. Multidisciplinary research group on diabetes of the instituto mexicano del seguros: glutathione peroxidase 3 serum levels and GPX3 gene polymorphisms in subjects with metabolic syndrome. *Arch Med Res*. 2014;45(5):375–382. doi:10.1016/j.arcmed.2014.05.001
38. Rega C, Russo R, Foca A, et al. Probing the interaction interface of the GADD45beta/MKK7 and MKK7/DTP3 complexes by chemical cross-linking mass spectrometry. *Int J Biol Macromol*. 2018;114:114–123. doi:10.1016/j.ijbiomac.2018.03.090
39. Wu S, Guo W, Chen L, et al. Downregulation of Gadd45beta alleviates osteoarthritis by repressing lipopolysaccharide-induced fibroblast-like synoviocyte inflammation, proliferation and migration. *Int Immunopharmacol*. 2024;126:111202. doi:10.1016/j.intimp.2023.111202
40. Schamberger AC, Schiller HB, Fernandez IE, et al. Glutathione peroxidase 3 localizes to the epithelial lining fluid and the extracellular matrix in interstitial lung disease. *Sci Rep*. 2016;6:29952. doi:10.1038/srep29952